Particle and Fibre Toxicology

RESEARCH Open Access

Iron oxide nanoparticles induce reversible endothelial-to-mesenchymal transition in vascular endothelial cells at acutely non-cytotoxic concentrations

Tao Wen[1†], Lifan Du[1†], Bo Chen[2], Doudou Yan[1], Aiyun Yang[1], Jian Liu[1], Ning Gu[3], Jie Meng[1*] and Haiyan Xu[1*]

Abstract

Background: Iron oxide nanoparticles (IONPs) have been extensively studied in different biomedical fields. Recently, the non-cytotoxic concentration of IONPs induced cell-specific response raised concern of their safety. Endothelial cell exposure was unavoidable in their applications, while whether IONPs affect the phenotype of vascular endothelial cells is largely unknown. In this work, the effect of IONPs on endothelial-to-mesenchymal transition (EndMT) was investigated in vitro and in vivo.

Results: The incubation with γ-Fe_2O_3 nanoparticles modified with polyglucose sorbitol carboxymethyether (PSC-Fe_2O_3) at non-cytotoxic concentration induced morphological changes of human umbilical vein endothelial cells (HUVECs) from cobblestone-like to spindle mesenchymal-like morphology, while PSC-Fe_2O_3 mostly stay in the culture medium and intercellular space. At the same time, the endothelial marker CD31 and VE-cadherin was decreased along with the inhibitory of angiogenesis properties of HUVEC. Meanwhile, the mesenchymal marker α-smooth muscle actin (α-SMA) and fibroblast specific protein (FSP) was up regulated significantly, and the migration ability of the cells was enhanced. When ROS scavenger mannitol or AA was supplemented, the EndMT was rescued. Results from the in vivo study showed that, expression of CD31 was decreased and α-SMA increased in the liver, spleen and kidney of mice given PSC-Fe_2O_3, and the density of collagen fibers in the liver sinusoid of mice was increased. The supplementary mannitol or AA could reverse the degree of EndMT in the tissues. Mechanistic study in vitro indicated that the level of extracellular hydroxyl radicals (·OH) was up regulated significantly by PSC-Fe_2O_3, which induced the response of intracellular ROS and resulted in the EndMT effect on HUVECs.

Conclusion: The PSC-Fe_2O_3 was capable of inducing EndMT in the endothelial cells at acutely non-cytotoxic dose due to its intrinsic peroxidase-like activity, though they were few taken up by endothelial cell. The EndMT effect on HUVEC can be rescued by ROS scavenger in vitro and in vivo.

Keywords: Iron oxide nanoparticle, Endothelial-to-mesenchymal transition, Reactive oxygen species, Reversible

Background

Iron oxide nanoparticles (IONPs) have been intensively investigated and developed in many biomedical fields, such as intravenous cell targeting, labeling and separation, magnetic resonance imaging contrast, drug or gene delivery system, and hyperthermia [1–3], because they show a low cytotoxicity in a quite large range of tested concentration [4, 5]. Nevertheless, potential effects of IONPs at non-cytotoxic concentrations on human health have been explored in recent years, especially on vascular endothelial cells, because blood vessel is one of the major barriers for INOPs intended to use as therapeutics and diagnostics. For examples, it was reported that IONPs exposure induced the elongated morphology and increased elastic modulus of endothelial cells [6, 7]. Even no cytotoxicity was detected, at low amount of IONPs, the endocrine and urea

* Correspondence: mengjie@ibms.pumc.edu.cn; xuhy@pumc.edu.cn
†Tao Wen and Lifan Du contributed equally to this work.
[1]Institute of Basic Medical Sciences, Chinese Academy of Medical Sciences & Peking Union Medical College, Beijing 100005, China
Full list of author information is available at the end of the article

transporter function, inflammatory responses, angiogenesis function of endothelial cells (ECs) were found to change [8]. The endothelial integrity was also reported to alter via interplay with barrier function and attenuation of cytoprotective and anti-inflammatory NO production at non-cytotoxic concentration of IONPs [9]. These cues imply possible effects of IONPs at non-cytotoxic concentration on the phenotype of ECs.

Endothelium to mesenchymal transition (EndMT) is one changed phenotype of endothelial cells that represents losing endothelial characteristics and gaining a mesenchymal phenotype [10], which have a significant role in some diseases, especially fibrosis in liver [11, 12], kidney [13], cardiac [14], and atherosclerosis [15], diabetes [16] and cancer [17]. It also has been documented that endothelial cells can undergo EndMT in certain physiological environmental stimulations including growth factor TGFβ [18], materials stiffness [19], and stretching stress [20]. Whether IONPs can induce EndMT is unknown and worthy to note.

In this work, whether γ-Fe_2O_3 nanoparticles modified with polyglucose sorbitol carboxymethyether (PSC-Fe_2O_3) were able to inducing EndMT upon human umbilical vein endothelial cells (HUVECs) was investigated in vitro and in vivo. We showed that PSC-Fe_2O_3 at acutely non-cytotoxic concentration significantly reduced the expression of endothelial marker CD31 and VE-cadherin, meanwhile increased the mesenchymal marker α-smooth muscle actin (α-SMA) and fibroblast specific protein (FSP) due to the peroxidase-like activity, by which the migration of endothelial cells was enhanced and their angiogenic function was inhibited, clearly indicating the occurrence of EndMT in the endothelial cells. The underlying mechanism of PSC-Fe_2O_3 induced EndMT was also elucidated.

Results

Characterization and cytotoxicity of PSC-Fe_2O_3

The crystal core of PSC-Fe_2O_3 was about 10 nm in diameter (Fig. 1a), and the average hydrodynamic diameter was 58 nm with − 30 mV of zeta potential. It should be noted that PSC-Fe_2O_3 did not show any cytotoxicity to HUVECs when its concentration was reached at 600 μg/mL (Fig. 1b), however, the morphology of the cells changed significantly, showing a spindle mesenchymal-like morphology at the concentration while losing their endothelial characteristic polygonal shape (Fig. 1c). The ratio of length to diameter (L/D) for the endothelial cells was two folds of that of control group when incubated with 600 μg/mL PSC-Fe_2O_3 (Fig. 1d). When observed at a lower confluence of 70% after PSC-Fe_2O_3 treatment, HUVECs also became spindle mesenchymal-like morphology (Additional file 1: Figure S1).

PSC-Fe_2O_3 induce EndMT

Next we investigated what happened on the phenotype of HUVECs when their morphology changed largely. The expression of CD31 and VE-cadherin (VE-cad) was examined by immunoblotting and immunofluorescence upon HUVECs incubated with PSC-Fe_2O_3 at different concentrations. It was shown that the level of VE-cad was down regulated when PSC-Fe_2O_3 was at 300 μg/mL or 600 μg/mL, and CD31 was decreased as well when PSC-Fe_2O_3 was reached 600 μg/mL, while the expression of α-SMA and FSP significantly increased in the tested concentrations (Fig. 2a, b). These results clearly indicated that PSC-Fe_2O_3 was capable of inducing endothelial cell transformation to mesenchymal cells (EndMT) process at the acutely non-cytotoxic concentration.

PSC-Fe_2O_3 mainly stayed in the culture medium and intercellular space

To understand how EndMT was triggered by PSC-Fe_2O_3, we first examined whether PSC-Fe_2O_3 were internalized by HUVECs. Results from Prussian blue Staining showed little blue color was observed in the cytoplasm of HUVEC incubated with PSC-Fe_2O_3, only sparkle of blue staining was seen between the cells when PSC-Fe_2O_3 was at 600 μg/mL (Fig. 3a), suggesting few PSC-Fe_2O_3 were internalized. With TEM, no appreciable PSC-Fe_2O_3 was observed inside the cells; instead, a small part of PSC-Fe_2O_3 located in the intercellular space of the cells (Fig. 3b), and most of PSC-Fe_2O_3 (more than 99%) stayed in the culture medium, which was determined by phenanthroline spectrophotometric method. To further validate above observations, cell lysates were prepared by two procedures and the iron content of the lysates was determined by phenanthroline method (Fig. 3c). It was shown that as for the samples prepared by lysis only (procedure I), the iron content of PSC-Fe_2O_3 groups was significantly higher than that of control group and concentration dependent. While for the samples prepared by the lysis following trypsin digestion (procedure II), no difference of iron content was observed between the control group and the two PSC-Fe_2O_3 groups (Fig. 3d). Because the trypsin digestion made the cells disconnected, therefore the increased iron content in lysates of procedure I was attributable to the PSC-Fe_2O_3 locating in the intercellular space. At the same time, the results provided further evidence of few PSC-Fe_2O_3 were taken up.

Extracellularly PSC-Fe_2O_3 induced ROS increase by peroxidase-like activities

Internalized nanoparticles usually up-regulate intracellular ROS [21, 22]. Although PSC-Fe_2O_3 mainly located in the culture medium and intercellular space instead of being taken up by endothelial cells, the impact of PSC-

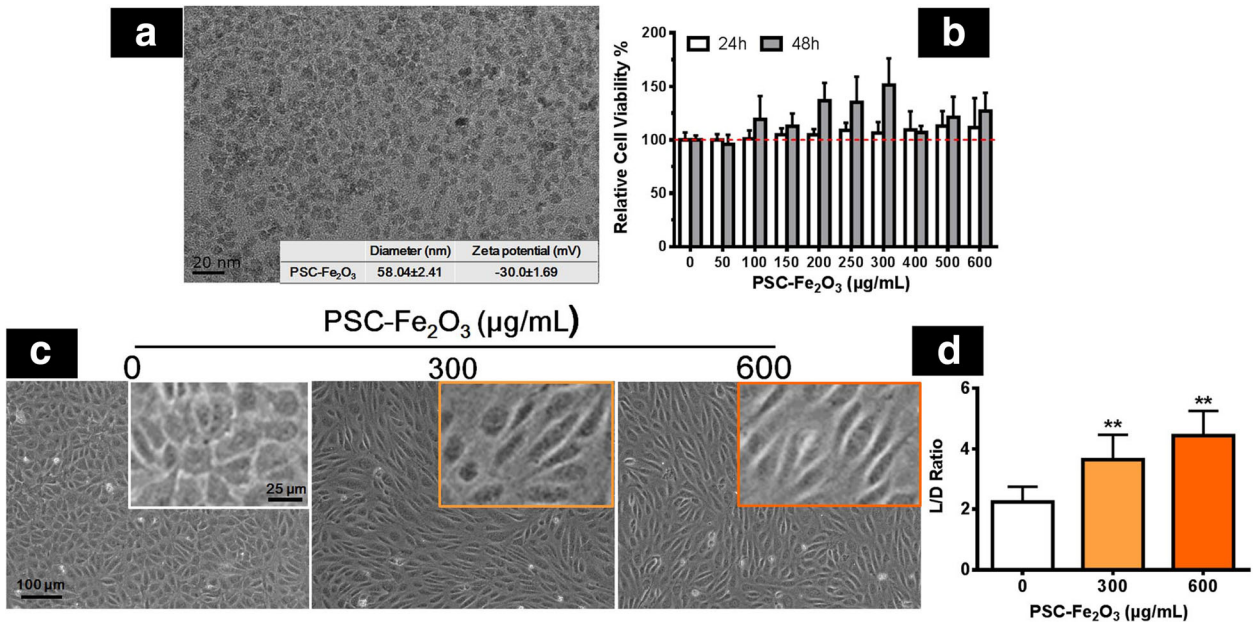

Fig. 1 **a** TEM image of PSC-Fe_2O_3, inserted provided the average dynamic diameter and Zeta potential of PSC-Fe_2O_3 in water. **b** Cell viability of HUVECs treated with PSC-Fe_2O_3 at different concentrations ($n = 3$). **c** Representative morphology of HUVECs treated with PSC-Fe_2O_3 at 300 and 600 μg/mL. **d** The average L/D ratio of HUVECs treated with different concentration of PSC-Fe_2O_3 ($n = 30$). Data are mean ± SD, one-way ANOVA with Dunnett's multiple comparisons test, ** $p < 0.01$, significant compared to control

Fe_2O_3 on the intracellular ROS was also examined. It was striking that the intracellular ROS of HUVECs was increased when incubated with PSC-Fe_2O_3, and the effect was in concentration dependent manner (Fig. 4a). We also examined the change of ROS stress marker *HO-1* at gene level. Results showed that the expression of *HO-1* was increased in dose-dependent manner when HUVECs were exposed with PSC-Fe_2O_3 (Fig. 4b), which confirmed that ROS played a key role in PSC-Fe_2O_3-induced EndMT. At the same time, the extracellular ROS was increased and H_2O_2 content decreased (Fig. 4b, c), which was concentration dependent too. It has been documented that IONPs is capable of decomposing H_2O_2 into hydroxyl radicals (·OH) due to its peroxidase-like activity [23], we next accessed the peroxidase-like activity of PSC-Fe_2O_3 upon the commonly used peroxidase colorimetric substrates o-phenylenediamine (OPD) in the presence of H_2O_2 [24]. As Fig. 4d proved, PSC-Fe_2O_3 catalyzed H_2O_2 into ·OH in a concentration dependent manner, showing the peroxidase property. Furthermore, we detected ·OH directly by electron spin resonance (ESR) spectroscopy with the help of a spin trap 5, 5-Dimethyl-1-pyrroline N-oxide (DMPO). The ESR spectrum of the spin adduct DMPO/·OH showed four lines with relative intensities of 1:2:2:1 and hyperfine splitting parameters of $a_N = 13.56$, $a_H^\beta = 12.30$, and $a_H^\gamma = 0.66$ [25] (Fig. 4f), which provided evidence that there was increased ·OH in the extracellular environment. Taken together above, we demonstrated that extracellular PSC-Fe_2O_3 decomposed H_2O_2, which resulted in the production of extracellular ·OH that induced up-regulation of intracellular ROS.

ROS scavengers reverse EndMT of HUVEC

Some reports suggested that the up-regulation of intracellular ROS was one crucial factor inducing EndMT [26, 27], therefore we next investigated the relationship between the EndMT and IONP-induced ROS. It was shown that the supplement of hydroxyl radicals (·OH) scavenger mannitol [28] or non-specific ROS scavenger ascorbic acid (AA) [29] was capable of reducing the intracellular ROS level of HUVECs incubated with PSC-Fe_2O_3 (Fig. 5a). Moreover, either mannitol or AA was able to increase the expression of VE-Cad and CD31 while to decrease α-SMA and FSP for HUVEC in the presence of PSC-Fe_2O_3 (Fig. 5b and c). Although the change was not large at each immunoblots, the CD31 was decreased by PSC-Fe_2O_3 at 600 μg/mL with statistical significance (Additional file 1: Figure S2A and B). To confirm this in further, we conducted additional experiments to investigate the change of CD31 from gene level. It was shown that CD31 was down regulated in the present of 600 μg/mL PSC-Fe_2O_3 and could be rescued by adding AA (Additional file 1: Figure S2C). These results strongly suggested that PSC-Fe_2O_3 induced extracellular ·OH was one crucial factor for the

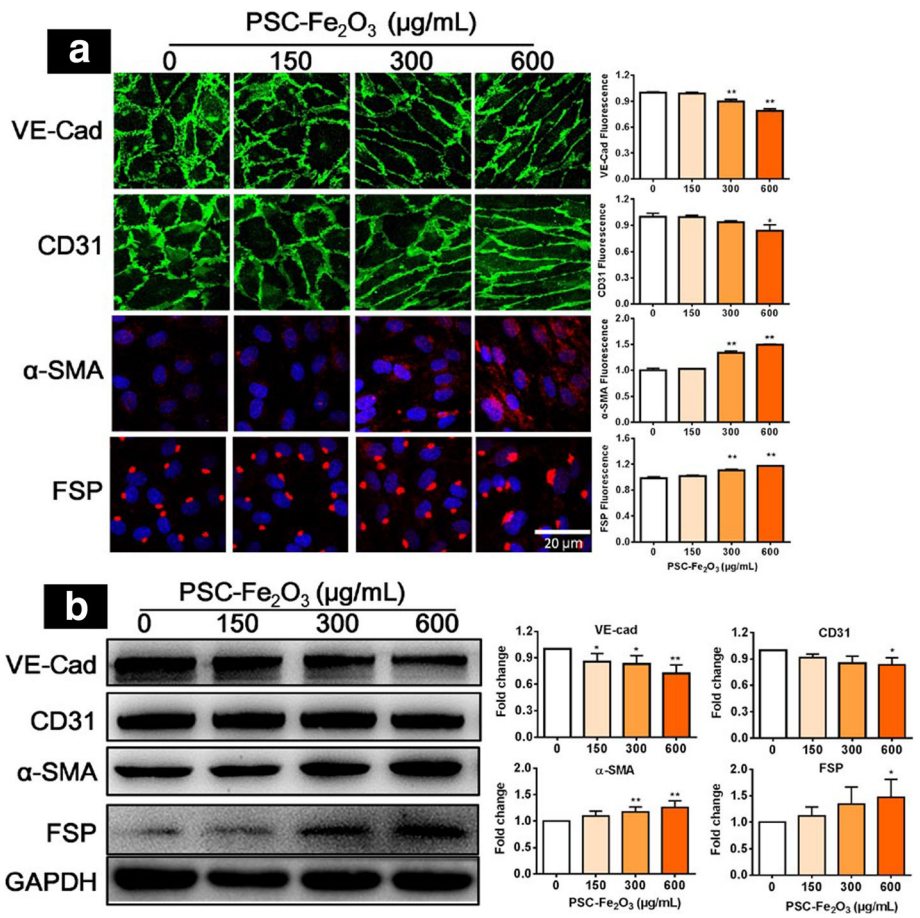

Fig. 2 PSC-Fe_2O_3 at non-cytotoxic concentration induced EndMT in HUVECs. **a** Representative fluorescence confocal microphotographs and quantitative fluorescence intensity of HUVECs immunostatined with endothelial cell marker CD31 (green) or VE-cadherin (green) and mesenchymal marker α-SMA (red) or FSP (red), counterstained with DAPI for nuclei (blue). **b** Representative immunoblots and quantification of CD31, VE-cadherin, α-SMA, FSP of protein lysates from HUVECs treated with PSC-Fe_2O_3. Data are mean ± SD, n = 3, one-way ANOVA with Dunnett's multiple comparisons test, *$p < 0.05$, ** $p < 0.01$, significant compared to control

occurrence of EndMT, which could be scavenged by the supplement of antioxidants.

As EndMT can inhibit the function of angiogenesis and promote invasion for endothelial cells [30, 31], we examined the ability of HUVECs to form vessel-like structures in the presence of PSC-Fe_2O_3. The observation under microscope showed that the tubules formed by control HUVECs were dense, complete and continuous, while those formed by HUVECs incubated with PSC-Fe_2O_3 were less, only sparse network and few branches were observed. When supplemented with AA, the HUVECs incubated with PSC-Fe_2O_3 recovered their angiogenic ability, evidenced by the increased tubule formation (Fig. 6a). Quantification results showed that the number of meshes was significantly different between control group and PSC-Fe_2O_3 group, and between PSC-Fe_2O_3 group and PSC-Fe_2O_3 with AA group (Fig. 6b). At the same time, the covering rate of wound scratch was faster for PSC-Fe_2O_3 group than that for the control group, indicating the function of migration and invasion of the cells was enhanced, and which could also be reverted by adding AA (Fig. 6c, d).

ROS scavengers rescued PSC-Fe_2O_3 induced EndMT in vivo

The EndMT induced by PSC-Fe_2O_3 was further investigated in healthy Balb/c mice. The mice were divided into four groups: control, PSC-Fe_2O_3 alone, PSC-Fe_2O_3 plus mannitol intravenously, and PSC-Fe_2O_3 intravenously plus AA oral administration. The exposure dose and routine were chosen according to the results in vitro and the references [4, 32]. Results obtained from the immunofluorescence staining showed that the expression of CD31 was decreased and α-SMA increased in the liver, kidney and spleen of mice given PSC-Fe_2O_3 alone, while the addition of mannitol or AA rescued the level of the two markers, which clearly indicated that oxidative stress induced by PSC-Fe_2O_3 could induce EndMT

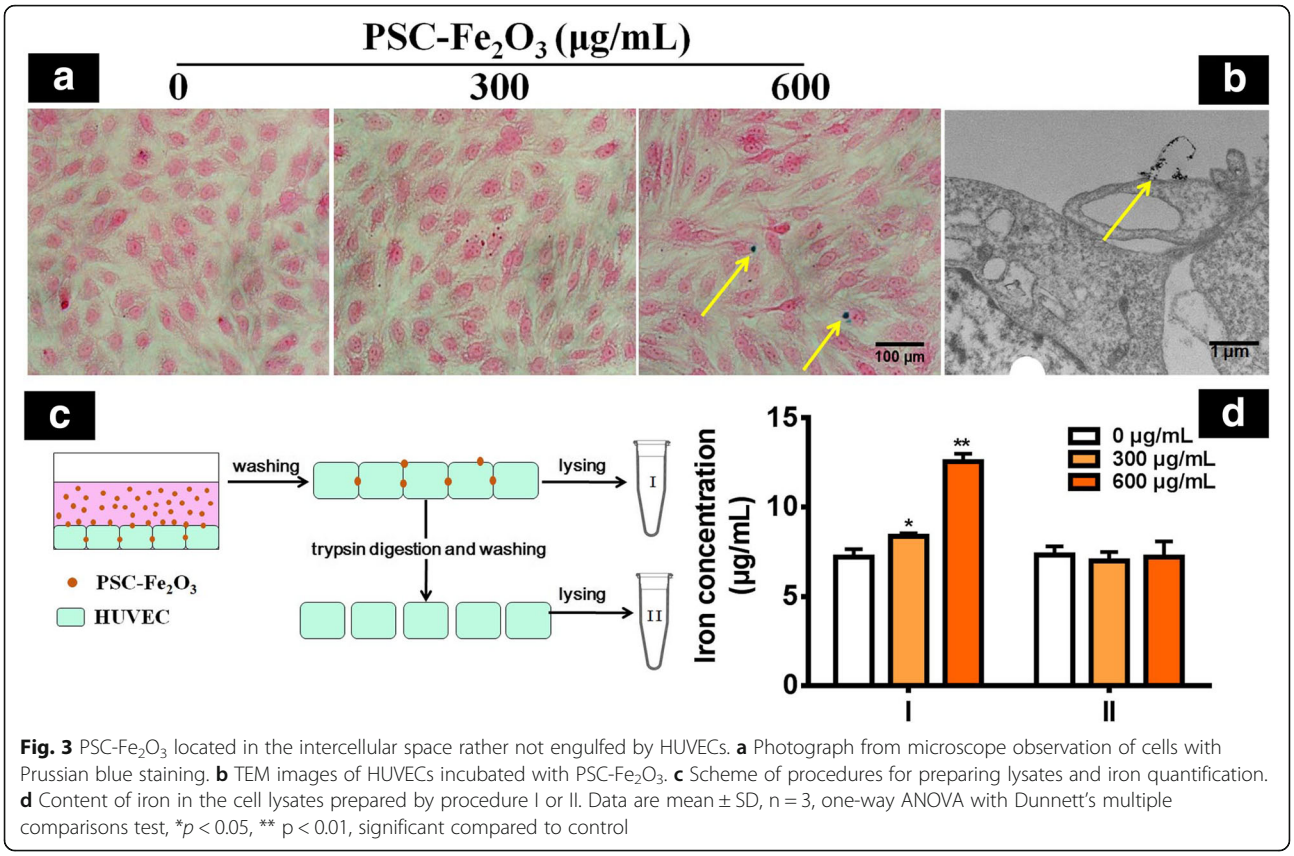

Fig. 3 PSC-Fe_2O_3 located in the intercellular space rather not engulfed by HUVECs. **a** Photograph from microscope observation of cells with Prussian blue staining. **b** TEM images of HUVECs incubated with PSC-Fe_2O_3. **c** Scheme of procedures for preparing lysates and iron quantification. **d** Content of iron in the cell lysates prepared by procedure I or II. Data are mean ± SD, n = 3, one-way ANOVA with Dunnett's multiple comparisons test, *$p < 0.05$, ** $p < 0.01$, significant compared to control

in those organs, and the effect was rescued by the use of ROS scavengers (Fig. 7). The immunohistochemical staining with the liver tissue also provided side evidence of down regulation for CD31 and upregulation for α-SMA (Additional file 1: Figure S3), which was consistent with the result of immunofluorescence staining. As shown in previous reports, either human microvascular endothelial cell (HMVEC) or liver sinusoidal endothelial cells (LSEC) underwent leakiness through the disruption of VE-cad when exposed to titanium dioxide nanoparticles [33, 34], which suggested endothelial cells from different sources have some features in common.

In addition, results from Masson's trichrome staining showed that the density of collagen fibers in the liver sinusoid of mice administrated with PSC-Fe_2O_3 alone was increased, which indicated the occurrence of liver fibrosis. The supplements of mannitol or AA could reduce the density of collagen fibers (Fig. 8).

Discussion

Endothelial-to-mesenchymal transition (EndMT) is accompanied with a progressive loss of endothelial markers and cell-to-cell adhesion, transition towards a mesenchymal phenotype, and enhancement on cell migration and invasion, which has been recognized to play a diverse role in many diseases, such as fibrosis, systemic sclerosis, diabetes and malignancy [10]. In this work, we revealed that PSC-Fe_2O_3 could induce EndMT at acutely non-cytotoxic concentration. In order to figure out whether the occurrence of EndMT came from the modification of PSC, we also performed experiments with bare Fe_2O_3 nanoparticles (bare-Fe_2O_3) of 10 nm in diameter (Additional file 1: Fig. S4A). The bare-Fe_2O_3 showed 50% of viability when the concentration was reached 300 μg/mL (Additional file 1: Figure S4B), and induced significant morphological changes of HUVECs, cells shape changed from polygonal to spindle at different concentrations less than 300 μg/mL (Additional file 1: Figure S4C). Different from the cellular uptake of PSC-Fe_2O_3, the bare-Fe_2O_3 was able to be engulfed by HUVECs evidenced by the increasing blue color in the cells. In further, western blot analysis showed that α-SMA was increased remarkably and VE-cad decreased at the same time in dose-dependent manner (Additional file 1: Figure S4D). These results indicated that bare-Fe_2O_3 was capable of inducing EndMT on HUVECs as well, suggesting that the induction of EndMT was closely related with the intrinsic property of NPs instead of surface modification and cellular uptake. Note, both PSC-Fe_2O_3 and bare-Fe_2O_3 were household, which should not be taken as equal ones to commercial products in application, considering that they may have

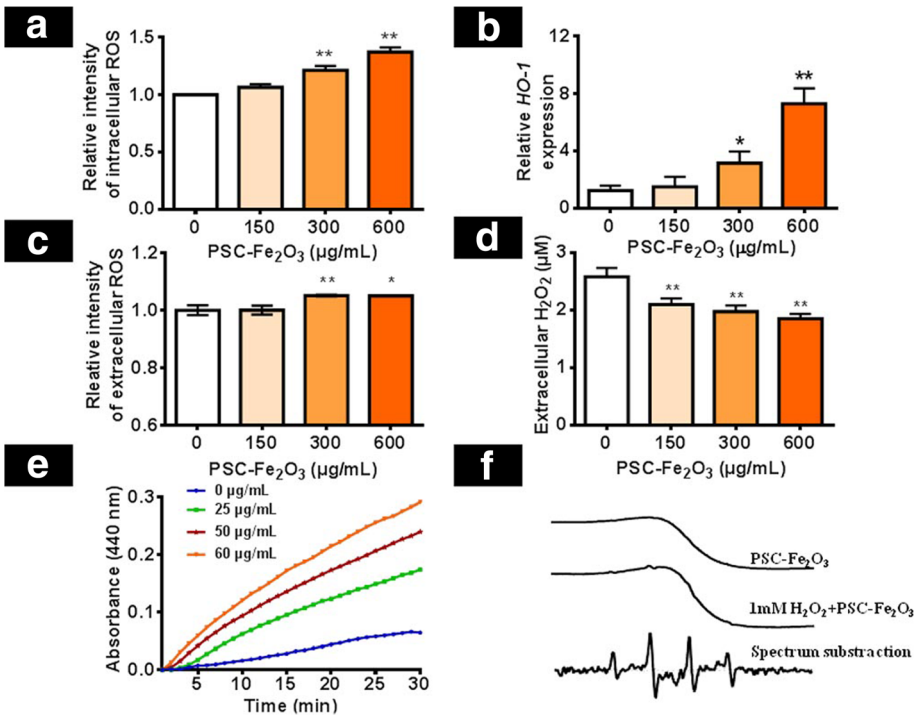

Fig. 4 PSC-Fe_2O_3 induced ·OH production by peroxidase-like activities. **a** Intracellular ROS of HUVEC. **b** HO-1 gene expression of HUVEC. **c** Extracellular ROS of HUVEC. **d** Extracellular H_2O_2. **e** PSC-Fe_2O_3 catalyzed H_2O_2 into ·OH in a concentration dependent manner. **f** The ESR spectrum of DMPO / ·OH adduct. Data are mean ± SD, n = 3, one-way ANOVA with Dunnett's multiple comparisons test, *$p < 0.05$, **$p < 0.01$, significant compared to control

different physicochemical properties. It was known that EndMT is a subtype of epithelial-mesenchymal transition (EMT). Several nanoparticles or nanostructures have been demonstrated to be able to induce EMT with epithelial cell in the pulmonary system or cancer cell, such as carbon nanotube [35–38], cerium oxide [39], titanium dioxide (TiO_2) [40], silica (SiO_2) [41], silver NPs [42], which is supportive to our observations on PSC-Fe_2O_3-induced EndMT. These insights about PSC-Fe_2O_3-induced EndMT can also provide a new view to evaluate the potential health risk of this nanoparticle in further applications.

IONPs are able to induce the production of intracellular ROS because they are internalized by cells and located in the lysosomes where the microenvironment is acidic [43]. Due to the surface modification, PSC-Fe_2O_3 were not engulfed by HUVECs, instead, they mainly adhered to the cell membrane or stayed in the intercellular space. Nevertheless, PSC-Fe_2O_3 were still capable of up-regulating the level of intracellular ROS by catalyzing extracellular H_2O_2 into ·OH that further induced oxidative stress of the cells and affected intracellular environment. Therefore we suggested that the intrinsic peroxidase-like activity of PSC-Fe_2O_3 brought out the EndMT effect. According to the mechanism, it was reasonable to consider that ROS scavengers could reverse the effect, which was validated by this study in vitro and in vivo. It was also important and encouraging to see that the supplementary of mannitol or AA could reduce the degree of EndMT, which implied that the combination of antioxidants with PSC-Fe_2O_3 was a promising way of prevention the risk of EndMT related toxicology for the pre- and clinical application with PSC-Fe_2O_3. Moreover, it was noticed that iron oxide nanoparticles could reduce the adherens conjugation between HUVECs and led to endothelial leakiness through increasing the production of ROS [21], which might be one of the potential mechanisms that trigger the occurrence of EndMT mediated by PSC-Fe_2O_3.

Conclusion

The peroxidase-like activity of PSC-Fe_2O_3 resulted in the up-regulation of intracellular ROS though they were mainly stay in the culture medium and intercellular space, which induced EndMT on HUVECs with the decreased level of CD31 and VE-cadherin, and increased expression of α-SMA and FSP. ROS scavenger mannitol or AA could rescue the EndMT induced by PSC-Fe_2O_3 in vitro and in vivo. These results provided a new insight into the potential toxicity of PSC-Fe_2O_3 on vascular endothelial cells and demonstrated ROS scavenge was

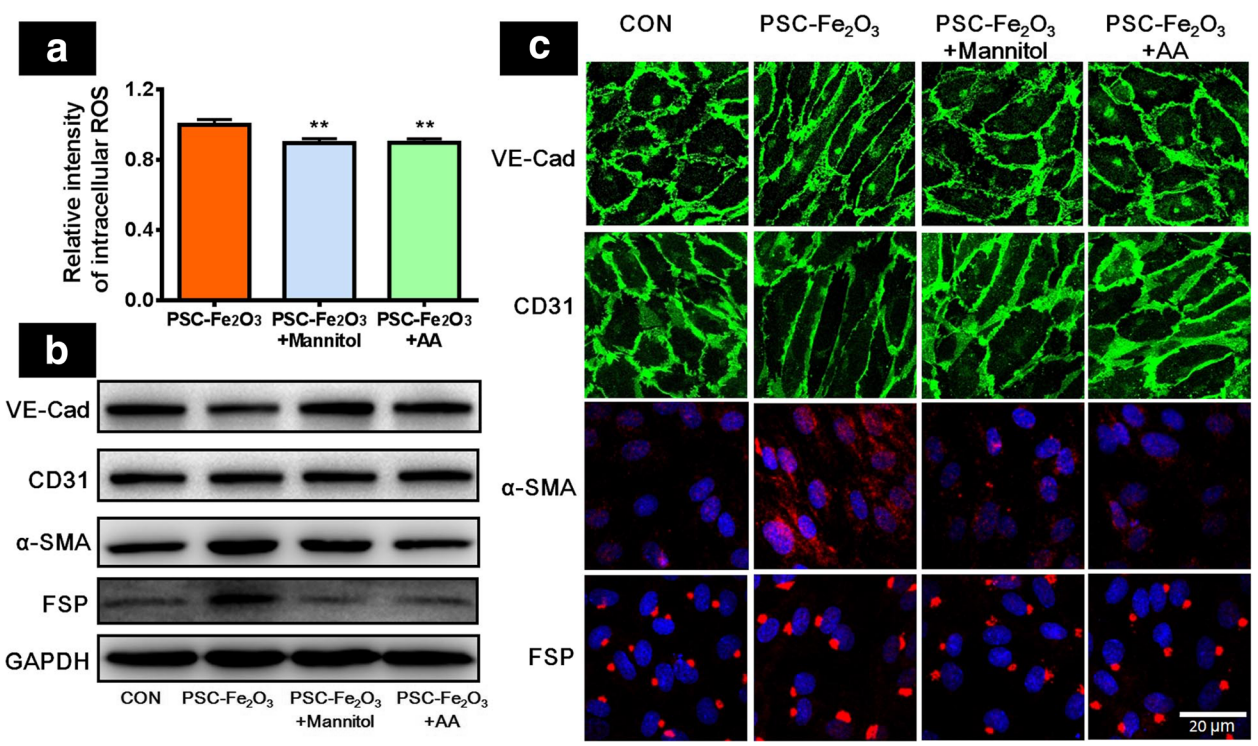

Fig. 5 ROS scavengers rescued the EndMT induced by PSC-Fe_2O_3. **a** Intracellular ROS of PSC-Fe_2O_3 treated HUVECs in the absence and presence of mannitol or AA. **b** The level of VE-cad, CD31, α-SMA and FSP determined by western blot. **c** Expression of VE-cad (green), CD31 (green), α-SMA (red) and FSP (red) for HUVECs by confocal microscopy. Data are mean ± SD, n = 3, one-way ANOVA with Fisher's least significant difference test (LSD-t), ** $p < 0.01$, significant compared to control

an effective strategy to reverse the process and reduce the potential toxicity.

Methods

PSC-Fe2O3 synthesis and characterization

The polydextrose sorbitol carboxymethyl ether (PSC) coated γ-Fe_2O_3 nanoparticles (PSC-Fe_2O_3) were synthetized by alternating-current magnetic field inducing method [44]. Bare Fe_2O_3 nanoparticles were prepared similar to PSC-Fe_2O_3 in the absent of PSC. The morphology of Fe_2O_3 was observed by transmission electron microscope (TEM-1400plus, JEOL). The hydrodynamic diameters and Zeta potential of PSC-Fe2O3 were detected by a Zetasizer Nano ZS90 analyzer (Malvern). Each measurement was repeated four times.

Cell culture

Human umbilical vein endothelial cells (HUVECs, #8000), endothelial cell medium (ECM, #1001), fetal bovine serum (FBS, #0025), penicillin/streptomycin solution (P/S, #0503), endothelial cell growth supplement (ECGS,#1052) and Poly-L-Lysine (PLL, #0403) were all purchased from ScienCell Research Laboratories (San Diego, CA). HUVECs were grown on PLL coated culture plate in ECM supplemented with 5% FBS, 1% P/S and 1% ECGS.

Cell viability assay

The viability of HUVECs incubated with Fe2O3 was analyzed using a cell count kit (CCK-8, Dojindo). The Fe2O3 was diluted in fresh medium to yield a final iron concentration that ranged from 0 to 600 μg/mL. After 24 h or 48 h incubation, the cells were rinsed twice with PBS and incubated with medium containing 10 μL CCK-8 reagents for 2 h. The absorbance of the medium was measured at 450 nm using a microplate reader (BioTek Synergy4). All measurements were carried out in triplicate, and the cell viability was calculated with the protocol provided by the manufacture.

Cell morphology assay

HUVEC cells were exposed to 0, 300 and 600 μg/mL PSC-Fe_2O_3. After 48 h, the morphology of cells was observed by the microscope (Olympus IX71). The length and diameter of thirty cells in each treatment was measured by ImageJ software, and the ratio of length to diameter (L/D) was calculated.

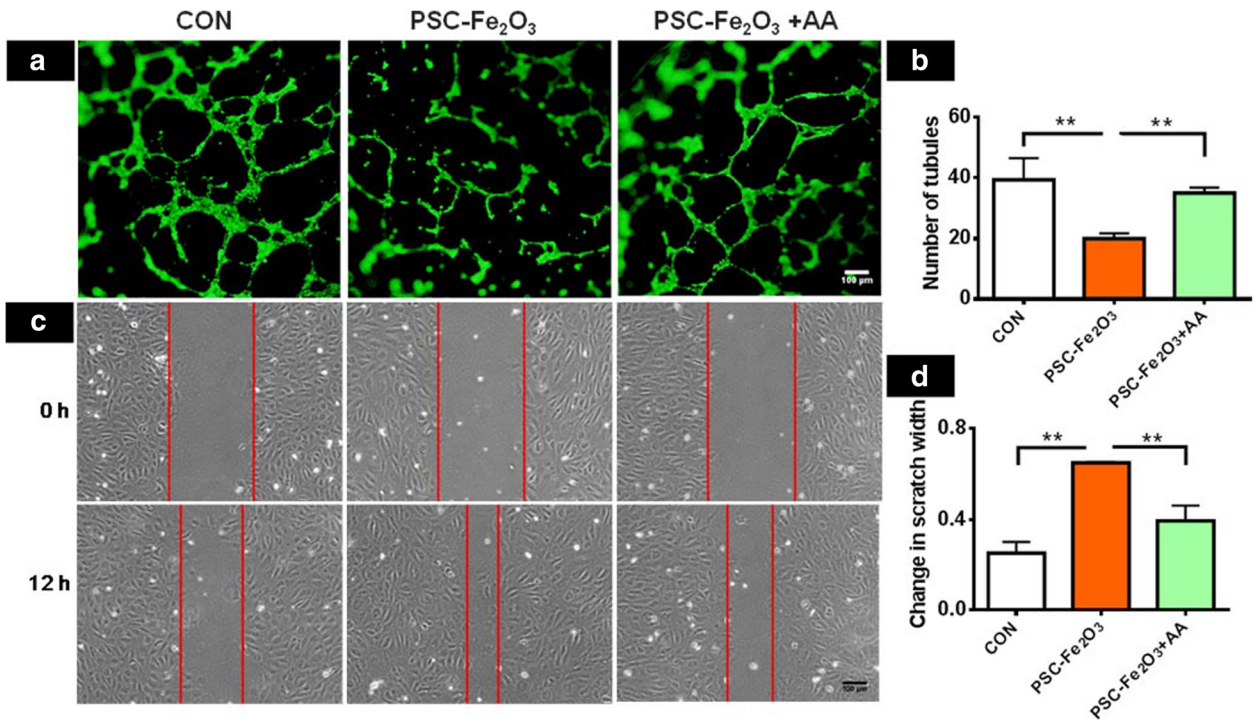

Fig. 6 ROS scavenger AA reversed the function of endothelial cells occurring EndMT. **a** AA reversed tubule formation impairment of endothelial cell caused by PSC-Fe_2O_3. **b** Quantification of endothelial meshes ($n = 3$). **c** Images of scratch morphology changing with time. **d** Relative scratch width change ($n = 2$). Data are mean ± SD, one-way ANOVA with LSD-t, ** $p < 0.01$. Bar is 100 μm for all images

Immunoblotting

Cells were incubated with 0, 150, 300 and 600 μg/mL Fe_2O_3 for 48 h at 37 °C. HUVECs were lysed in RIPA buffer and analyzed by western blot. Primary antibodies were as follows: anti-VE-cadherin (#2500S, Cell Signaling Technology, Danvers, MA), anti-CD31 (#3528, CST), anti-α-smooth muscle actin (#19245S, CST), anti-FSP (#13018, CST) and anti-GAPDH (sc-25778, Santa Cruz). Protein bands were quantified using ImageJ software. For the rescue experiment, HUVECs were co-cultured by Fe_2O_3 with 0.88 mg/mL mannitol or 8.8 mg/mL ascorbic acid (AA).

Immunofluorescent staining

Cells were treated with different concentrations of PSC-Fe_2O_3 for 48 h and then fixed with 4% paraformaldehyde for 15 min. After rinsing with PBS, cells were incubated with blocking solution (1% bovine serum albumin (BSA) in PBS with 0.3% Triton) for 1 h at room temperature. The following primary antibodies were applied overnight at 4 °C: anti-VE-cadherin, anti-CD31, anti-α-smooth muscle actin, and anti-FSP. Cells were washed with PBS, and corresponding fluorescent secondary antibodies (CST) were applied for 1 h at room temperature. Nuclear staining was performed use 4′, 6-diamidino-2-phenylindole (DAPI, Zhongshan Goldenbridge). Micrographs were taken by the FluoView FV1000 confocal microscope (Olympus), and analyzed with ImageJ software. For the rescue experiment, the cells were treated with 600 μg/mL PSC-Fe_2O_3 and 0.88 mg/mL mannitol or 8.8 mg/mL AA. The paraffin-embedded liver, spleen, and renal sections were deparaffinized with xylene. After treatment with 3% BSA for 30 min, sections were incubated overnight with primary CD31 and α-SMA antibody. Slides were then washed and incubated in the dark for 50 min with corresponding alexa fluor® 488 or CY3 labeled secondary antibody. Slides were then again washed in PBS and counterstained with DAPI-containing mounting medium.

Tubule formation

Cells were pretreated with 600 μg/mL PSC-Fe_2O_3 in the absent or present of 50 mM AA for 48 h before seeded in matrigel coated 96-well plates. Cells were allowed to attach for 8 h, stained with Calcien AM (Molecular Probe) and photographed by the fluorescence microscope (Olympus, IX71). Numbers of tubules were quantified using ImageJ with the Angiogenesis Analyzer plugin. Data presented were from three independent experiments.

Wound-healing assay

Cells were pretreated with 600 μg/mL PSC-Fe_2O_3 with or without 50 mM AA for 48 h and then starved without

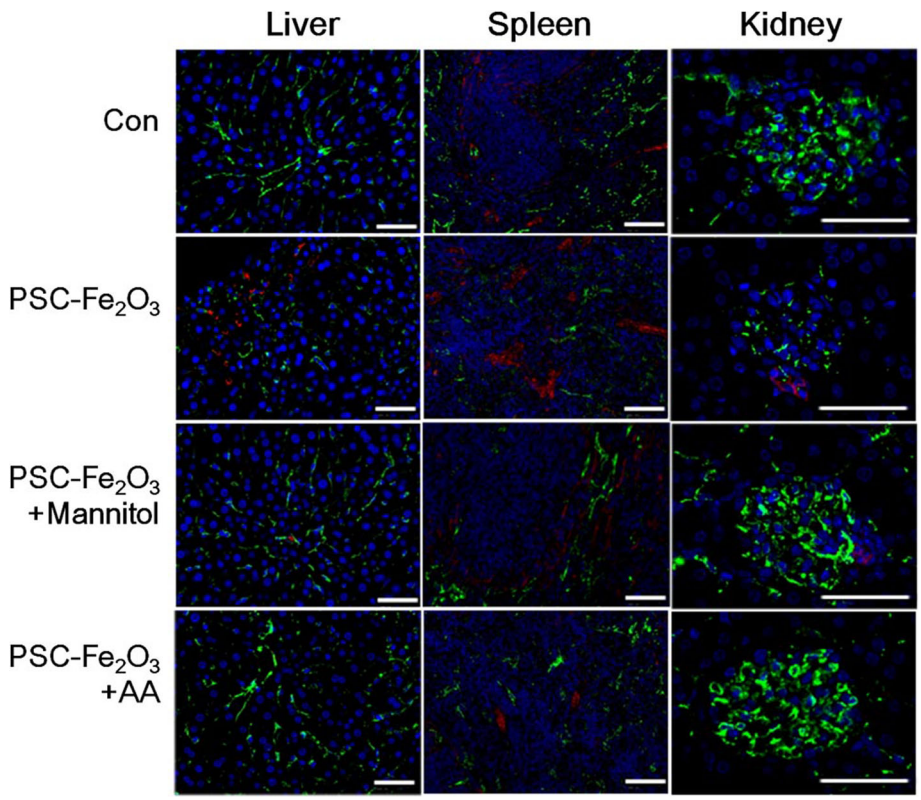

Fig. 7 Representative of liver, spleen and kidney sections stained for mesenchymal markers α-SMA (red), the endothelial markers CD31 (Green), and nuclei (blue). Bar is 50 μm for all images

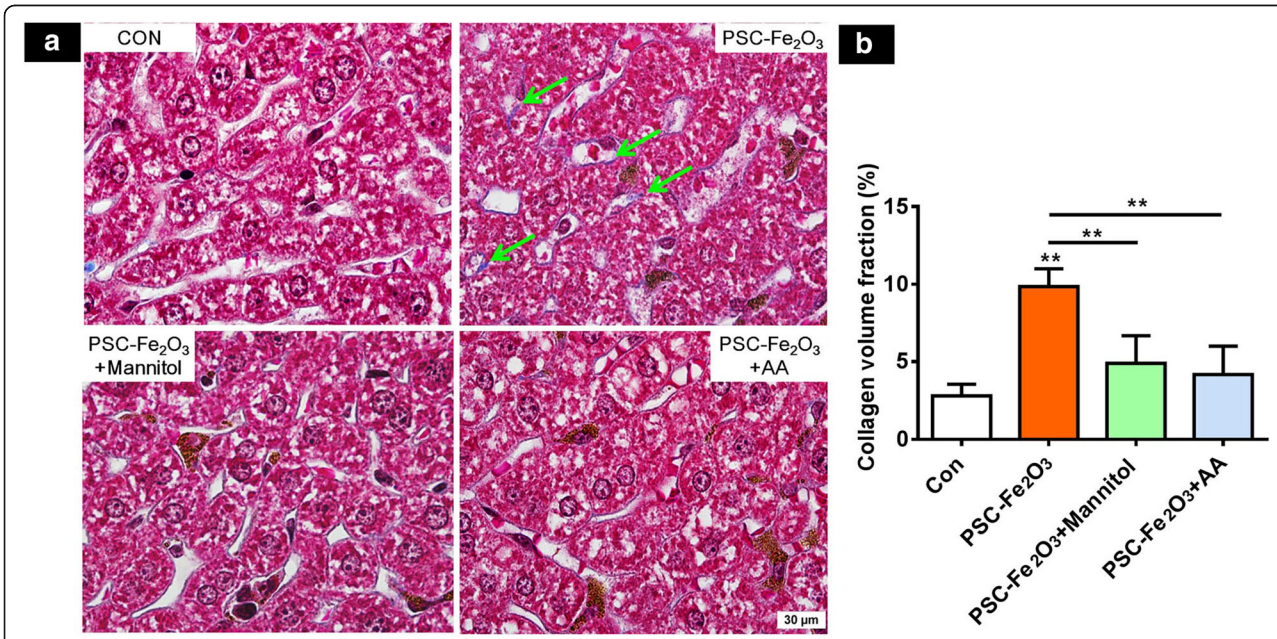

Fig. 8 a Representative images of liver sections with Masson's trichrome staining (blue color pointed by green arrows) for extracellular matrix collagen. **b** Quantification of collagen volume fraction. Data are mean ± SD, $n = 4$, one-way ANOVA with LSD-t, *$p < 0.05$, ** $p < 0.01$

FBS for 12 h. Wounds were made with 200 μL sterile pipette tip and washed with PBS to eliminate non adherent cells, thus a wound approximate 165 μm was created. Then cells were cultured with medium with 0.5% FBS and images were acquired at 0 and 12 h (Olympus IX71). Movements of cells were calculated using ImageJ software. The changes of scratch width were calculated with initial wound width subtracted to that of 12 h and then divided by the initial one.

Prussian blue staining

Cells were treated with different concentrations of Fe_2O_3 for 48 h. After removing the culture medium, the cells were washed with PBS for three times and fixed with 4% paraformaldehyde for 30 min. The fixed cells were incubated with Prussian blue solution containing 5% hydrochloric acid aqueous solution and 5% potassium ferrocyanide (II) trihydrate for 30 min to determine the intracellular iron followed by staining with nuclear fast red. The cells were placed on an inverted microscope for observation.

Transmission electron microscopy (TEM)

Cells were treated with 600 μg/mL PSC-Fe_2O_3 for 48 h and then detached with trypsin and fixed overnight with 2.5% glutaraldehyde at 4 °C. The samples were then postfixed in Osmium (VIII) tetroxide (OsO_4), dehydrated in ethanol, and embedded in Epon (Fluka). Sections were cut with an ultra-microtome and placed on copper grids for observation (TEM-1400 plus, JEOL).

Iron content measurements

Cells were treated with PSC-Fe_2O_3 for 48 h. There are two different procedures to deal with HUVECs before detecting the iron content in cells. Procedure I: the cells were washed with PBS and lysed by 100 μL RIPA. Procedure II: the cells washed with PBS were detached from the plates with trypsin and collected by centrifugation, and then washed with PBS and lysed by 100 μL RIPA. The amount of iron was quantified with phenanthroline spectrophotometric method [45]. The iron content in the culture medium was determined with the same method. Standard calibration of iron amount and absorbance at 510 nm was built by using series concentration (0, 20, 40, 60, 80, 100 μg/mL) of $FeCl_3$ solution. The concentrations of iron in the lysates and medium were calculated from the standard curve. Data presented were from three independent experiments performed in triplicate.

Intracellular reactive oxygen species (ROS) measurement

The intracellular ROS level was measured using the probe 2′,7′-dichlorodihydrofluorescein diacetate (DCFH-DA, Sigma-Aldrich). HUVECs were treated with various concentration of PSC-Fe_2O_3 for 24 h and the culture supernatant was collected. The cells were then washed with PBS for three times. Cells were incubated with 10 μM DCFH-DA for 30 min and then digested and collected. The fluorescence intensity was detected by flow cytometer (BD Accuri C6). For the rescue experiment, the cells were treated by PSC-Fe_2O_3 with 0.88 mg/mL mannitol or 8.8 mg/mL AA. Data presented were from three independent experiments performed in triplicate.

Extracellular H_2O_2 and ROS measurement

The extracellular H_2O_2 and ROS level was measured using the above collected supernatants. In order to avoid interference from PSC-Fe_2O_3, ultrafiltration centrifugal filter (10 K, Amicon®) was used to separate PSC-Fe_2O_3 from supernatants. Centrifugal filter was performed following the manufacturer's recommendations. In short, the supernatants were added to the device, followed by centrifugation. Then, the solution in the filter collection tube was collected.

The H_2O_2 concentration in the filtered solution was detected by hydrogen peroxide assay Kit (Beyotime Biotechnology). Standard calibration of H_2O_2 was built by using series concentration (1, 2, 5, 10, 20 μM) of H_2O_2 solution (Beijing Chemical Works) with absorbance at 560 nm. The concentration of H_2O_2 in the filtered solution was calculated with the standard curve. Data from three independent experiments were presented.

To explore the effect of PSC-Fe_2O_3 on extracellular ROS production, we used a modified assay with DCFH-DA probe [46]. DCFH-DA in DMSO was hydrolyzed in NaOH aqueous solution for 30 min to yield DCFH intermediate. The obtained DCFH solution was neutralized with NaH_2PO_4 and shielded from light. The obtained filtered supernatants were mixed with DCFH solution. After 30-min incubation, the fluorescence was detected (BioTek Synergy4) and the excitation and emission wavelengths were set at 488 and 525 nm, respectively.

qPCR

Cells were incubated with 0, 150, 300 and 600 μg/mL PSC-Fe_2O_3 for 24 h at 37 °C. The total RNA of the cells was extracted by using trizol (MKCB2851V, Sigma) with one-step extraction. Total RNA was transcribed using the cDNA synthesis kit (#RR036A, TaKaRa). Quantitative real-time-PCR (qPCR) was performed using the real-time PCR system (Bio-Rad) and TB Green fluorescein mix (#RR420A, TaKaRa). Data were normalized based on GAPDH expression as housekeeping gene. All primers were synthesized from TSINGKE Biological Technology and shown in Table 1.

Table 1 Sequences information of the gene primers

	Forward	Reverse
HO-1	AAGACTGCGTTCCTGCTCAAC	AAAGCCCTACAGCAACTGTCG
GAPDH	GTCAAGCTCATTTCCTGGT	CCAGGGTTTCTTACTCCTTG

In vitro peroxidase-like activity assay

The peroxidase-like activity of PSC-Fe_2O_3 was evaluated in deionized water with the catalytic oxidation of o-phenylenediamine (OPD). The peroxidase-like activities of different concentrations (0, 25, 50, 60 μg/mL) PSC-Fe_2O_3 were employed with 45 μg/mL OPD and 370 mM H_2O_2. The progress was monitored with UV-vis-NIR spectrophotometer (PerkinElmer Lambda 950) with 1-min intervals at 440 nm. All operations were done at room temperature and in the dark.

Electron spin resonance (ESR)

Hydroxyl radicals (·OH) can be detected by ESR with the help of the spin trap 5,5-Dimethyl-1-pyrroline N-oxide (DMPO, Dojindo). The ESR measurements were carried out using a Magnettech ESR spectrometer (MS-5000) at ambient temperature. 50 μL aliquots of control or sample solutions were taken in quartz capillary tubes. Other settings were as follows: 2 G field modulation, 100 G scan range, and 10 mW microwave power.

Animal experiments

Animal experiments were carried out in accordance with a protocol that was approved by the Institutional Animal Care and Use committee (Institute of Basic Medical Sciences, Chinese Academy of Medical Sciences, and Peking Union Medical College). Female Balb/c mice (average weight 20 g) were maintained at the institutional experimental animal center under specific pathogen-free conditions. The mice were fed with sterilized food and autoclaved tap water.

Mice were divided into four groups, and each group consisted of three mice. Mice were intravenous injection of PSC-Fe_2O_3 or in combination with mannitol or oral administration AA as the following table showed (Table 2).

The mice were treated once a day for 7 days and then sacrificed. The tissues were collected and fixed in 4% parformaldehyde for 24 h and subsequently embedded in paraffin for histopathological and immunohistochemistry analysis.

Table 2 The administration procedure of mice

Group	Intragastrical administration (100 μL)	intravenous injection (100 μL)
Control	saline	saline
PSC-Fe_2O_3	saline	4 mg/mL PSC-Fe_2O_3
PSC-Fe_2O_3 + AA	40 mg/mL AA	4 mg/mL PSC-Fe_2O_3
PSC-Fe_2O_3 + mannitol	saline	4 mg/mL PSC-Fe_2O_3 + 5.87 mg/mL mannitol

Note: saline was 0.9% sodium chloride

Histopathological and immunohistochemistry analysis

The paraffin-embedded tissue sections were deparaffinized with xylene. Endogenous peroxidase was blocked with 0.3% H_2O_2 for 25 min. After treatment with 3% BSA for 30 min, sections were incubated overnight with primary CD31 and α-SMA antibody. Slides were then washed and incubated with a horse radish peroxidase-linked secondary antibody for 50 min at room temperature, followed by diaminobenzidine and counterstaining with Mayer's hematoxylin.

The slides were stained with Masson's trichrome for evaluation of interstitial collagen deposition. Collagen area and total tissue area were measured using ImageJ and the IHC Tool Box plugin. Collagen volume fraction (CVF) was calculated dividing collagen area by the total area. For each group, four replicates were counted and calculated.

Statistical analysis

The data are shown as mean ± standard deviation (SD) for all treatment groups. Statistical significance was ascertained through one way ANOVA with SPSS software (SPSS17.0).

Additional file

Additional file 1: Figure S1. Representative morphology of low density of HUVECs treated with 300 and 600 μg/mL PSC-Fe_2O_3. **Figure S2.** PSC-Fe_2O_3 inhibited CD31 protein and gene expression, which was rescued by antioxidants. (A) Three replications of CD31 immunoblots. (B) Quantification of CD31 expression for HUVECs with different treatments. (C) Gene expression of CD31 for endothelial cell with different treatments. Data are mean ± SD, one-way ANOVA with LSD-t, ** $p < 0.01$. **Figure S3.** Representative of liver sections stained for mesenchymal markers α-SMA, and the endothelial markers CD31. **Figure S4.** Effects of bare Fe_2O_3 nanoparticles (bare-Fe_2O_3) on HUVECs. (A) TEM image for bare-Fe_2O_3. (B) Cell viability of HUVECs treated with different concentrations of bare-Fe_2O_3 for 24 h or 48 h. (C) Representative immunoblots of VE-Cadherin and α-SMA of HUVECs treated with 0, 10, 50 and 300 μg/mL of bare-Fe_2O_3 for 48 h. (D) Microscope observation of HUVEC cells treated with different concentrations of bare-Fe_2O_3 after Prussian blue staining. (DOCX 1010 kb)

Abbreviations

AA: ascorbic acid; DCFH-DA: 2′, 7′-dichlorodihydrofluorescein diacetate; DMPO: 5, 5-Dimethyl-1-pyrroline N-oxide; ECs: Endothelial cell; EndMT: Endothelial-to-mesenchymal transition; ESR: Electron spin resonance; FSP: Fibroblast specific protein; HUVEC: Human umbilical vein endothelial cells; IONPs: Iron oxide nanoparticles; OH: Hydroxyl radicals; OPD: o-phenylenediamine; PSC-Fe_2O_3: γ-Fe_2O_3 nanoparticle core and polyglucose sorbitol carboxymethyether shell; ROS: Reactive oxygen species; TEM: Transmission electron microscope; α-SMA: α-smooth muscle actin

Acknowledgements

Not applicable.

Consent of publication
Not applicable.

Authors' contributions
TW, JM, and HYX designed experiments and made data analysis and wrote the main manuscript. LFD conducted main experiments and prepared data for Figs. BC provided the PSC-Fe_2O_3 and related data. TW, JM, DDY and AYY took part in part of the experiments. TW, JM, JL, NG and HYX discussed part sections of the manuscript. All authors reviewed the manuscript. All authors read and approved the final manuscript.

Funding
The work was supported by the National Key R&D Program of China (2017YFA0205504), CAMS Innovation Fund for Medical Science (CIFMS 2016- I2M-3-004 and 2018-I2M-3-006), and the National Natural Science Foundation of China (31771005 and 81801771).

Availability of data and materials
The datasets used and/or analysed during the current study are available from the corresponding author on reasonable request.

Ethics approval and consent to participate
Animal experiments were carried out in accordance with a protocol that was approved by the Institutional Animal Care and Use committee (Institute of Basic Medical Sciences, Chinese Academy of Medical Sciences, and Peking Union Medical College, China). Female Balb/c mice were maintained at the institutional experimental animal center under specific pathogen-free conditions. The mice were fed with sterilized food and autoclaved tap water.

Competing interests
The authors declare that they have no competing interests.

Author details
[1]Institute of Basic Medical Sciences, Chinese Academy of Medical Sciences & Peking Union Medical College, Beijing 100005, China. [2]Materials Science and Devices Institute, Suzhou University of science and Technology, Suzhou 215009, China. [3]State Key Laboratory of Bioelectronics, Jiangsu Key Laboratory for Biomaterials and Devices, School of Biological Science and Medical Engineering, Southeast University, Nanjing 210096, China.

Received: 22 March 2019 Accepted: 7 July 2019
Published online: 12 July 2019

References
1. Cardoso VF, Francesko A, Ribeiro C, Banobre-Lopez M, Martins P, Lanceros-Mendez S. Advances in magnetic nanoparticles for biomedical applications. Adv Healthc Mater. 2018;7:5.
2. Hu Y, Mignani S, Majoral JP, Shen M, Shi X. Construction of iron oxide nanoparticle-based hybrid platforms for tumor imaging and therapy. Chem Soc Rev. 2018;47(5):1874–900. https://doi.org/10.1039/C7CS00657H.
3. Duan M, Shapter JG, Qi W, Yang S, Gao G. Recent progress in magnetic nanoparticles: synthesis, properties, and applications. Nanotechnology. 2018;29(45):452001. https://doi.org/10.1088/1361-6528/aadcec.
4. Valdiglesias V, Kilic G, Costa C, Fernandez-Bertolez N, Pasaro E, Teixeira JP, et al. Effects of iron oxide nanoparticles: cytotoxicity, genotoxicity, developmental toxicity, and neurotoxicity. Environ Mol Mutagen. 2015;56(2):125–48. https://doi.org/10.1002/em.21909.
5. Feliu N, Docter D, Heine M, Del Pino P, Ashraf S, Kolosnjaj-Tabi J, et al. In vivo degeneration and the fate of inorganic nanoparticles. Chem Soc Rev. 2016;45(9):2440–57. https://doi.org/10.1039/C5CS00699F.
6. Buyukhatipoglu K, Clyne AM. Superparamagnetic iron oxide nanoparticles change endothelial cell morphology and mechanics via reactive oxygen species formation. J Biomed Mater Res A. 2011;96(1):186–95. https://doi.org/10.1002/jbm.a.32972.
7. Buyukhatipoglu K. Flame synthesis and in vitro biocompatibility assessment of superparamagnetic Iron oxide nanoparticles: cellular uptake, toxicity and proliferation studies. J Nanoscience Nanotechnol. 2009;9:12.
8. Ge G, Wu H, Xiong F, Zhang Y, Guo Z, Bian Z, et al. The cytotoxicity evaluation of magnetic iron oxide nanoaprticles on human aortic endothelial cells. Nanoscale Res Lett. 2013;8:215. https://doi.org/10.1186/1556-276X-8-215.
9. Astanina K, Simon Y, Cavelius C, Petry S, Kraegeloh A, Kiemer AK. Superparamagnetic iron oxide nanoparticles impair endothelial integrity and inhibit nitric oxide production. Acta Biomater. 2014;10(11):4896–911. https://doi.org/10.1016/j.actbio.2014.07.027.
10. Kovacic JC, Mercader N, Torres M, Boehm M, Fuster V. Epithelial-to-mesenchymal and endothelial-to-mesenchymal transition: from cardiovascular development to disease. Circulation. 2012;125(14):1795–808. https://doi.org/10.1161/CIRCULATIONAHA.111.040352.
11. Dufton NP, Peghaire CR, Osuna-Almagro L, Raimondi C, Kalna V, Chuahan A, et al. Dynamic regulation of canonical TGFbeta signalling by endothelial transcription factor ERG protects from liver fibrogenesis. Nat Commun. 2017;8:895.
12. Ribera J, Pauta M, Melgar-Lesmes P, Cordoba B, Bosch A, Calvo M, et al. A small population of liver endothelial cells undergoes endothelial-to-mesenchymal transition in response to chronic liver injury. Am J Physiol Gastrointest Liver Physiol. 2017;313(5):G492–504. https://doi.org/10.1152/ajpgi.00428.2016.
13. Jourde-Chiche N, Fakhouri F, Dou L, Bellien J, Burtey S, Frimat M, et al. Endothelium structure and function in kidney health and disease. Nat Rev Nephrol. 2019;15(2):87–108. https://doi.org/10.1038/s41581-018-0098-z.
14. Zeisberg EM, Tarnavski O, Zeisberg M, Dorfman AL, McMullen JR, Gustafsson E, et al. Endothelial-to-mesenchymal transition contributes to cardiac fibrosis. Nat Med. 2007;13(8):952–61. https://doi.org/10.1038/nm1613.
15. Wesseling M, Sakkers TR, de Jager SCA, Pasterkamp G, Goumans MJ. The morphological and molecular mechanisms of epithelial/endothelial-to-mesenchymal transition and its involvement in atherosclerosis. Vasc Pharmacol. 2018;106:1–8. https://doi.org/10.1016/j.vph.2018.02.006.
16. Shi Y, Vanhoutte PM. Macro- and microvascular endothelial dysfunction in diabetes. J Diabetes. 2017;9(5):434–49. https://doi.org/10.1111/1753-0407.12521.
17. Potenta S, Zeisberg E, Kalluri R. The role of endothelial-to-mesenchymal transition in cancer progression. Br J Cancer. 2008;99(9):1375–9. https://doi.org/10.1038/sj.bjc.6604662.
18. Dejana E, Hirschi KK, Simons M. The molecular basis of endothelial cell plasticity. Nat Commun. 2017;8:14361.
19. Zhang H, Chang H, Wang LM, Ren KF, Martins MC, Barbosa MA, et al. Effect of polyelectrolyte film stiffness on endothelial cells during endothelial-to-mesenchymal transition. Biomacromolecules. 2015;16(11):3584–93. https://doi.org/10.1021/acs.biomac.5b01057.
20. Shoajei S, Tafazzoli-Shahdpour M, Shokrgozar MA, Haghighipour N. Alteration of human umbilical vein endothelial cell gene expression in different biomechanical environments. Cell Biol Int. 2014;38(5):577–81. https://doi.org/10.1002/cbin.10237.
21. Apopa PL, Qian Y, Shao R, Guo NL, Schwegler-Berry D, Pacurari M, et al. Iron oxide nanoparticles induce human microvascular endothelial cell permeability through reactive oxygen species production and microtubule remodeling. Part Fibre Toxicol. 2009;6:1. https://doi.org/10.1186/1743-8977-6-1.
22. Chou CC, Chen W, Hung Y, Mou CY. Molecular elucidation of biological response to mesoporous silica nanoparticles in vitro and in vivo. ACS Appl Mater Interfaces. 2017;9(27):22235–51. https://doi.org/10.1021/acsami.7b05359.
23. Gao L, Zhuang J, Nie L, Zhang J, Zhang Y, Gu N, et al. Intrinsic peroxidase-like activity of ferromagnetic nanoparticles. Nat Nanotechnol. 2007;2(9):577–83. https://doi.org/10.1038/nnano.2007.260.
24. Jiang B, Duan D, Gao L, Zhou M, Fan K, Tang Y, et al. Standardized assays for determining the catalytic activity and kinetics of peroxidase-like nanozymes. Nat Protoc. 2018;13(7):1506–20. https://doi.org/10.1038/s41596-018-0001-1.
25. Zhao H, Joseph J, Zhang H, Karoui H, Kalyanaraman B. Synthesis and biochemical applications of a solid cyclic nitrone spin trap: a relatively superior trap fo detecting superoxide anions and glutathiyl radicals. Free Radic Biol Med. 2001;31(5):599–606. https://doi.org/10.1016/S0891-5849(01)00619-0.
26. Suzuki T, Tada Y, Nishimura R, Kawasaki T, Sekine A, Urushibara T, et al. Endothelial-to-mesenchymal transition in lipopolysaccharide-induced acute lung injury drives a progenitor cell-like phenotype. Am J Physiol Lung Cell Mol Physiol. 2016;310(11):L1185–98. https://doi.org/10.1152/ajplung.00074.2016.
27. Huynh DL, Zhang JJ, Chandimali N, Ghosh M, Gera M, Kim N, et al. SALL4 suppresses reactive oxygen species in pancreatic ductal adenocarcinoma phenotype via FoxM1/Prx III axis. Biochem Biophys Res Commun. 2018;503(4):2248–54. https://doi.org/10.1016/j.bbrc.2018.06.145.
28. Gao L, Liu R, Gao F, YalingWang JX, Gao X. Plasmon-Mediated Generation of Reactive Oxygen Species from Near-Infrared Light Excited Gold Nanocages for Photodynamic Therapy in Vitro. ACS Nano. 2014;8(7):7260–71. https://doi.org/10.1021/nn502325j.

29. Dave RI, Shah NP. Effectiveness of ascorbic acid as an oxygen scavenger in improving viability of probiotic bacteria in yoghurts made with commercial starter cultures. Int Dairy J. 1997;7(6–7):435–43.
30. Coll-Bonfill N, Musri MM, Ivo V, Barberà JA, Tura-Ceide O. Transdifferentiation of endothelial cells to smooth muscle cells play an important role in vascular remodelling. Am J Stem Cells. 2015;4(1):13–21.
31. Patel J, Baz B, Wong HY, Lee JS, Khosrotehrani K. Accelerated endothelial to mesenchymal transition increased fibrosis via deleting notch signaling in wound vasculature. J Invest Dermatol. 2018;138(5):1166–75. https://doi.org/10.1016/j.jid.2017.12.004.
32. Zhou Q, Wei Y. For better or worse, Iron overload by superparamagnetic Iron oxide nanoparticles as a MRI contrast agent for chronic liver diseases. Chem Res Toxicol. 2017;30(1):73–80.
33. Setyawati MI, Tay CY, Chia SL, Goh SL, Fang W, Neo MJ, et al. Titanium dioxide nanomaterials cause endothelial cell leakiness by disrupting the homophilic interaction of VE-cadherin. Nat Commun. 2013;4:1673.
34. Tee JK, Ng LY, Koh HY, Leong DT, Ho HK. Titanium Dioxide Nanoparticles Enhance Leakiness and Drug Permeability in Primary Human Hepatic Sinusoidal Endothelial Cells. Int J Mol Sci. 2018;20(1):35.
35. Polimeni M, Gulino GR, Gazzano E, Kopecka J, Marucco A, Fenoglio I, et al. Multi-walled carbon nanotubes directly induce epithelial-mesenchymal transition in human bronchial epithelial cells via the TGF-beta-mediated Akt/GSK-3beta/SNAIL-1 signalling pathway. Part Fibre Toxicol. 2016;13(1):27. https://doi.org/10.1186/s12872-019-1042-2.
36. Chang CC, Tsai ML, Huang HC, Chen CY, Dai SX. Epithelial-mesenchymal transition contributes to SWCNT-induced pulmonary fibrosis. Nanotoxicology. 2012;6(6):600–10.
37. Chen T, Nie H, Gao X, Yang J, Pu J, Chen Z, et al. Epithelial-mesenchymal transition involved in pulmonary fibrosis induced by multi-walled carbon nanotubes via TGF-beta/Smad signaling pathway. Toxicol Lett. 2014;226(2):150–62. https://doi.org/10.1016/j.toxlet.2014.02.004.
38. Wang P, Wang Y, Nie X, Braini C, Bai R, Chen C. Multiwall carbon nanotubes directly promote fibroblast-myofibroblast and epithelial-mesenchymal transitions through the activation of the TGF-beta/Smad signaling pathway. Small. 2015;11(4):446–55. https://doi.org/10.1002/smll.201303588.
39. Ma J, Bishoff B, Mercer RR, Barger M, Schwegler-Berry D, Castranova V. Role of epithelial-mesenchymal transition (EMT) and fibroblast function in cerium oxide nanoparticles-induced lung fibrosis. Toxicol Appl Pharmacol. 2017;323:16–25. https://doi.org/10.1016/j.taap.2017.03.015.
40. Setyawati MI, Sevencan C, Bay BH, Xie J, Zhang Y, Demokritou P, et al. Nano-TiO2 Drives Epithelial-Mesenchymal Transition in Intestinal Epithelial Cancer Cells. Small. 2018;14(30):1800922. https://doi.org/10.1002/smll.201800922.
41. Yang M, Qian X, Wang N, Ding Y, Li H, Zhao Y, et al. Inhibition of MARCO ameliorates silica-induced pulmonary fibrosis by regulating epithelial-mesenchymal transition. Toxicol Lett. 2019;301:64–72. https://doi.org/10.1016/j.toxlet.2018.10.031.
42. Choo WH, Park CH, Jung SE, Moon B, Ahn H, Ryu JS, et al. Long-term exposures to low doses of silver nanoparticles enhanced in vitro malignant cell transformation in non-tumorigenic BEAS-2B cells. Toxicol in Vitro. 2016;37:41–9. https://doi.org/10.1016/j.tiv.2016.09.003.
43. Chen Z, Yin J-J, Zhou Y-T, Zhang Y, Song L, Song M, et al. Dual enzyme-like activities of Iron oxide nanoparticles and their implication for Diminishing Cytotoxicity. ACS Nano. 2012;6(5):4001–12. https://doi.org/10.1021/nn300291r.
44. Chen B, Li Y, Zhang X, Liu F, Liu Y, Ji M, et al. An efficient synthesis of ferumoxytol induced by alternating-current magnetic field. Materials Letters. 2016;170:93–6.
45. Hao S, Meng J, Zhang Y, Liu J, Nie X, Wu F, et al. Macrophage phenotypic mechanomodulation of enhancing bone regeneration by superparamagnetic scaffold upon magnetization. Biomaterials. 2017;140:16–25. https://doi.org/10.1016/j.biomaterials.2017.06.013.
46. Lin AH, Liu MH, Ko HK, Perng DW, Lee TS, Kou YR. Lung epithelial TRPA1 transduces the extracellular ROS into transcriptional regulation of lung inflammation induced by cigarette smoke: the role of Influxed Ca^{2+}. Mediat Inflamm. 2015;2015:148367.

Publisher's Note